Estimating the Medium Access Probability in Large Cognitive Radio Networks

Claudina Rattaro[a,*], Federico Larroca[a], Paola Bermolen[a], Pablo Belzarena[a]

[a] *Facultad de Ingeniería, Universidad de la República*
Julio Herrera y Reissig 565, ZC 11300, Montevideo, Uruguay

Abstract

During the last decade we have seen an explosive development of wireless technologies. Consequently the demand for electromagnetic spectrum has been growing dramatically resulting in the spectrum scarcity problem. In spite of this, spectrum utilization measurements have shown that licensed bands are vastly underutilized while unlicensed bands are too crowded. In this context, Cognitive Radio Network emerges as an auspicious paradigm in order to solve those problems. The main question that motivates this work is: what are the possibilities offered by cognitive radio to improve the effectiveness of spectrum utilization? With this in mind, we propose a methodology, based on configuration models for random graphs, to estimate the medium access probability of secondary users. We perform simulations to illustrate the accuracy of our results and we also make a performance comparison between our estimation and one obtained by a stochastic geometry approach.

Keywords: cognitive radio networks, random graphs, stochastic geometry, dynamic spectrum allocation, fluid limit

1. Introduction

The widely extended use of wireless technologies in our everyday lives (e.g. mobile phones, sensors, laptops), together with the prediction that the mobile data traffic will increase 8-fold between 2015 and 2020 [2], have shifted the attention and efforts of many researchers all over the world towards the study of Cognitive Radio Networks (see for example [27, 25, 24, 11]). This concept is not new, and was first introduced by Mitola [19] in 1999. Cognitive Radio represents a promising technology which, based on dynamic spectrum access, strives at solving two important problems: spectrum underutilization and spectrum scarcity.

In this paradigm we can identify two classes of users: primary and secondary. Primary users (PUs) are those for which a certain portion of the spectrum has been allocated to (often in the form of a paid contract). Secondary users (SUs) are devices which are capable of detecting unused licensed bands and adapt their transmission parameters for using them.

The fundamental concept behind Cognitive Radio Networks (CRNs) is to allow SUs to use the licensed resource in the absence of PUs in order to improve the spectrum utilization. The key requirement in this context is that the PUs ought to be as little affected as possible by the presence of SUs. In the ideal case, PUs would use the network without being affected at all by SUs, which will in turn make use of whatever resources are left available.

Let us define the Medium Access Probability (MAP) as the mean number of concurrent transmissions that take place in a network divided by the total number of nodes. Given the network and the PUs utilization, one of the main performance metrics of interest here is naturally the MAP of SUs. This value measures the portion of spectrum "wasted" by PUs and which may be leveraged by SUs.

Many works like [5, 6, 7, 17, 23] have demonstrated that mathematical techniques such as stochastic geometry [26] and random graphs [28, 9] are excellent tools in order to predict diverse wireless network performance metrics. They are specially useful to model interactions between nodes in large random networks. This randomness may include node positions, node mobility, fading, or traffic (stochastic arrivals and departure).

Stochastic geometry allows to study the average behavior over many spatial realizations of a network whose nodes are placed according to some spatial probability distribution. Generally, the location of the nodes are assumed to be a realization of an homogeneous Poisson point process (PPP). Moreover, and for particular cases, these probabilistic models may include other factors such as propagation models, transmitting power, receiving sensitive, antenna radiation patterns, signal polarization, and power/interference thresholds. The articles [21, 22, 18] are the most representative examples of the use of stochastic geometry in cognitive radio networks. The authors obtained closed formulas for bounds of some performance metrics (such as MAP) in different CRNs contexts. However, in some scenarios the obtained bounds are very conservative. Moreover, in more general cases (e.g. when the processes involved are not Poisson or when the fading variables are not independent), determining these bounds is a difficult task, if not impossible.

On the other hand, since we are interested in the MAP, many network characteristics (e.g. propagation models, trans-

*Corresponding author
Email addresses: crattaro@fing.edu.uy (Claudina Rattaro), flarroca@fing.edu.uy (Federico Larroca), paola@fing.edu.uy (Paola Bermolen), belza@fing.edu.uy (Pablo Belzarena)

mitting power, etc.) can be abstracted into a (random) graph. Vertices in the graph represent nodes (or links) of the wireless network, and two nodes (or links) are connected by an edge when they cannot transmit simultaneously (as a consequence of the medium access mechanism, or the spectrum sensing capabilities of SUs). Then, the study of these structures provides an alternative route in order to predict performance metrics such as the MAP. In particular, recently the authors of [8] proposed a methodology for very general random graphs (characterized by the node's degree distribution), and they proved that some key properties of the system can be captured by ordinary differential equations. Authors of [7] applied this method in a wireless environment (RTS/CTS CSMA network) and obtained accurate results in the estimation of the MAP, whereas the methodology was further refined and simplified in [10].

In this paper, we consider two large wireless networks, one composed by PUs and the other by SUs. We are interested in estimating the MAP of SUs. To this end, we choose an approach based on random graphs and we extend the methodology developed in [8, 10] to the context of CRNs. In particular, the main difficulties that arise in this work are related to the interaction between both networks. However, we show that the methodology yields differential equations for which explicit solutions may be obtained. With our proposal, we show that it is possible to calculate an analytic approximation of the MAP (both for PUs and, most importantly, SUs) in an arbitrary large heterogeneous random network.

As a further contribution of this article, we perform a comparison between the approximation presented here, based on random graphs, with that based on a stochastic geometry approach. To perform the comparison we will refer to [21], where the authors studied an analogous problem and they obtained a bound of the MAP of SUs. We also analyze how conservative this bound is in some representative scenarios. On the one hand, these comparisons will be performed on those scenarios where a stochastic geometry approach is valid and possible. On the other hand, we will show that the approach presented here is more general than the one that uses spatial models, analyzing their performance in real network scenarios (e.g. when the involved processes are not necessarily Poisson).

The rest of the paper is structured as follows. In section 2 we introduce our hypotheses and the main characteristics of the considered MAC protocol. In section 3 we present our main results, in particular we show the MAP estimation using a random graph approach based on [8]. In section 4 we validate our results presenting numerical examples in several scenarios. In section 5, we give an introduction of the stochastic geometric model proposed in [21] and we compare their results with our MAP approximation in representative cases. Finally, we conclude and discuss future work in section 6.

2. Context and Assumptions

This work bears on the analysis of a general scenario where there is a primary wireless network coexisting with a secondary one. In this context, SUs try to exploit the unused licensed spectrum, so the MAC protocol should provide mechanisms to give SUs a way to detect the primary spectrum holes.

In particular, we work with the Cognitive-CSMA model introduced in [21] where Carrier Sensing (CS) is used for spectrum sensing and for interference control. In this mechanism, the following principles are verified:

- each PU has a protection zone,
- no SU can transmit inside the protection zone of a PU,
- time is slotted,
- each time slot consists of three phases: primary sensing, secondary sensing and transmission.

During the primary sensing phase, all PUs sample an independent and identically distributed random variable that represents its backoff timer. When the time indicated by its backoff timer is elapsed, the tagged PU checks whether the channel is free (by means of the CS mechanism mentioned before), and if so immediately begins transmitting. In other words, a PU will transmit during a time-slot if and only if its timer is the smallest among all its primary contenders.

Once the primary phase is over, and the corresponding PUs are transmitting, the secondary sensing phase begins. Similarly to the previous phase, all SUs sample a backoff timer, after which time they transmit if the channel is free. The difference in this case is that the CS mechanism has to evaluate the presence of both SUs and, most importantly, PUs. Note that the protection zone of the PUs is thus implicitly defined by the ability of SU's CS mechanism to detect the presence of PUs. All in all, a SU will transmit if and only if it is not in the protection zone of an active primary user and its timer is the smallest among its secondary contenders. In this context, the MAP is defined as the probability that a user be granted the right to transmit in a time slot.

Naturally, the determination of the protection zone and contender transmitters is strongly related with the nodes' positions and propagation conditions (i.e. path-loss and fading variables). In our present context, and similarly to [21], we will assume that the CS will evaluate the channel as busy if the signal of any other node is received with an energy above a certain threshold. This threshold may be different for secondary and primary nodes.

Finally, and regarding traffic, we will assume that all SUs are saturated, i.e. have a packet ready to be sent in every time slot. This assumption stems from the fact that we are interested in estimating the capacity of SUs to exploit the resources left by the PUs (i.e. the MAP of SUs).

3. Random Graphs and Configuration Algorithm

3.1. Preliminaries and Motivation

As we mentioned above, at any time-slot, and given the nodes' position and propagation conditions, we may determine the protection zone of each PU and all contending nodes. This, together with the backoff timers, will in turn determine which

nodes will be allowed to transmit. Note however that what is actually required to determine which nodes will transmit is precisely which pairs of nodes are contenders, and which SUs are in the protection zone of each PU (as opposed to the complete nodes' position and detailed propagation conditions).

The discussion above suggests that the network may be abstracted to a graph $\mathscr{G}(\mathscr{V},\mathscr{E})$ (the so-called interference graph), where the set of vertices represent the primary and secondary nodes, and the edges model the interference between any two nodes. In other words, if a transmission of node s triggers the CS of node r, then an edge from node s to r will exist. Note that in the particular case where s is a PU and r a SU, then an edge will exist if r is in the protection zone of s.

We will further assume a symmetric channel among PUs and SUs, meaning that the edges between nodes of the same type of user are bidirectional. Note however that the edges between a PU and a SU are directional, since the former are not affected by the latter (in other words, connections from SUs to PUs are meaningless in this context). If an edge exists between two nodes, we say that those nodes are contenders (or neighbors).

Let us now discuss what information we have on $\mathscr{G}(\mathscr{V},\mathscr{E})$. For instance, if the network is relatively small and static, we may know the graph completely. If on the other hand, the network is very big, has varying propagation conditions, and/or transient or mobile nodes (which is probably the case for SUs), the most natural modeling tool is a random graph.

This in turn induces the question of what probabilistic model use in the construction of the graph. We may for instance expect that on average each PU will have k_{PP} primary neighbors, that k_{PS} SUs are on average on the protection zone of the typical PU, and that each SU has k_{SS} secondary neighbors on average. In this case a reasonable model would be a variation of the well-known Erdös-Rényi model [15], where for instance a link between any two primary nodes will exist with probability $\frac{k_{PP}}{N_P-1}$ (with N_P the total number of primary nodes).

We may further enrich our model if we have information regarding the distribution of the nodes' degree (and not just its mean as in the previous example). That is to say, we know the counting measure $\mu(i,j)$, representing the number of PUs which have i PU neighbors and j SUs in its protection zone. Furthermore, we also know $\nu(i,j)$, which will count the number of SUs that belong to the protection zone of i PUs, and that have j SUs neighbors (thus $\sum_{i,j} j\mu(i,j) = \sum_{i,j} i\nu(i,j)$). The example considered in the last paragraph may be cast to this context by considering $\mu(i,j)$ and $\nu(i,j)$ as two-dimensional binomial distributions. That is,

$$\mu(i,j) = N_P F_{bin}(N_P-1, p_{PP}, i) F_{bin}(N_S, p_{PS}, j)$$
$$\nu(i,j) = N_S F_{bin}(N_P, p_{PS}, i) F_{bin}(N_S-1, p_{SS}, j)$$

where $F_{bin}(n,p,i) = C_i^n p^i (1-p)^{n-i}$ and the probabilities are $p_{PP} = \frac{k_{PP}}{N_P-1}$, $p_{PS} = \frac{k_{PS}}{N_S}$ and $p_{SS} = \frac{k_{SS}}{N_S-1}$.

The analysis to calculate the resulting MAP may then be as follows: construct a random graph (randomly chosen from those which comply to the chosen counting measures), analyze the resulting CSMA algorithm on that particular graph, and then weight the result over all possible graphs. However, this naive approach will become impractical as soon as the number of nodes is relatively big. To circumvent this complication, the idea proposed in [8] (and refined in [10]) is to construct the graph at the same time as the nodes transmit. By smartly choosing the variables considered (as we will present in Sec. 3.3), a Markov Chain may be constructed such that, when the number of nodes is large, it may be studied by means of a system of differential equations.

The framework discussed above has two implicit approximations. The first one, is that the analysis is valid for an infinite number of nodes, making it valid for moderate to large networks. The second one, which will be clearer when we present with more detail the graph's construction below, is that the counting measures used in the abstraction do not include any spatial information (i.e. the correlation between degree of nodes). However, we will show by means of simulations that, as soon as fading is not negligible, the MAP estimated by means of the set of differential equations constitutes an excellent approximation (and it is still very good when this is not the case).

3.2. Configuration Model

Let us first focus on the primary sensing phase. As we mentioned before, each PU chooses a random backoff timer, at which time they will check whether the channel is free. This is equivalent to a random ordering of the PU nodes, meaning that any continuous distribution is equivalent for the backoff timer (in terms of the resulting order). We will thus choose, without loss of generality, an exponentially distributed backoff timer with mean equal to one.

The key to our analysis is the procedure by which the graph $\mathscr{G}(\mathscr{V},\mathscr{E})$ is constructed along with the CSMA algorithm: the so-called configuration model [20]. Please recall that we have N_P and N_S primary and secondary users respectively, and that our a priori information are the counting measures $\mu(i,j)$ and $\nu(i,j)$. In this construction, we start with a "disconnected" graph. By this we mean that we have a set $\mathscr{V}$ of N_P+N_S vertices where, for instance, we have $\mu(i,j)$ nodes with i primary and j secondary neighbors, but precisely which other nodes are these neighbors is not revealed until the tagged node transmits. In this sense, we will use the term half-edges to refer to these unmatched edges. The methodology considered here constructs $\mathscr{G}(\mathscr{V},\mathscr{E})$ by pairing the half-edges sequentially as nodes transmit.

Please note that each node has two types of half-edges: some that should be connected to primary nodes, and others that should be connected to secondary nodes. The pairing above should be performed with this in mind. For instance, a half-edge from a PU to a SU should be paired with a half-edge from a SU to a PU.

Let us consider a time t during the primary sensing phase. The set $\mathscr{V}$ may be partitioned into the following subsets:

1. Primary nodes that are already transmitting: $\mathscr{A}_t^P$ (active nodes).
2. Primary and secondary nodes that have been blocked by the ongoing primary transmissions: $\mathscr{B}_t^P$ and $\mathscr{B}_t^S$ (blocked nodes). These nodes will not transmit during this slot.

3. Primary and secondary nodes that are neither transmitting nor blocked: $\mathscr{E}_t^P$ and $\mathscr{E}_t^S$ (unexplored nodes). These are the nodes that may transmit in the future, and will become either active or blocked as the sensing phase advances.

When the slot has just begun, we have $\mathscr{A}_0^P = \emptyset$, $\mathscr{B}_0^S = \mathscr{B}_0^P = \emptyset$ and $|\mathscr{E}_0^P| = \sum_{i,j} \mu(i,j) = N_P$ and $|\mathscr{E}_0^S| = \sum_{i,j} \nu(i,j) = N_S$.

Assume that the backoff timer of a node s in $\mathscr{E}_t^P$ expires at time t. The following then occurs (see Figure 1 for a toy example):

1. s is moved from $\mathscr{E}_t^P$ to $\mathscr{A}_t^P$.
2. Each half-edge of s is in turn paired with another uniformly randomly chosen unmatched half-edge. This way, we construct a graph sampled at random and uniformly from all graphs that comply to the measures $\mu(i,j)$ and $\nu(i,j)$.
3. All vertices whose half-edges were chosen in the previous step, and which are still unexplored (some may already be blocked), are moved from $\mathscr{E}_t^P$ to $\mathscr{B}_t^P$ and from $\mathscr{E}_t^S$ to $\mathscr{B}_t^S$ respectively.

The primary sensing phase ends when $|\mathscr{E}_t^P| = 0$. Half-edges to and from primary nodes which are yet to be matched may be safely ignored, since they belong to blocked nodes.

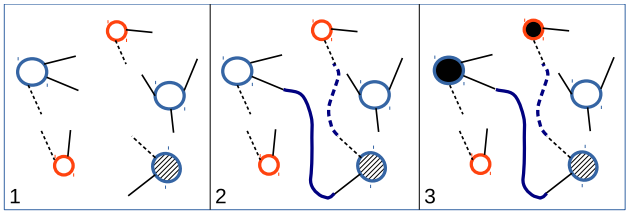

Figure 1: Illustration of primary sensing phase. In this toy example, there are represented three PUs (big blue circles) and two SUs (small red circles). Please see their half-edges that are all initially unpaired (solid half-edges will connect PU-PU or SU-SU, and dashed ones will connect PU-SU). In Step 1, a PUs is selected and become to be an active node (the hatched circle). This node has degree $(1,1)$ (one solid and one dashed half-edge respectively). This means that the node will have two neighbors: one primary and one secondary. In Step 2, each half-edge of the new active node is in turn paired with another uniformly randomly chosen unmatched half-edge. In other words, in this step the neighbors of the hatched node are defined. Finally, the nodes (PUs and SUs) which are neighbors of the active node (the ones which their half-edges were chosen in step 2) are moved to the blocked set (black nodes).

The secondary sensing phase thus begins, which is very similar to what we described before. The most important difference is that we have to consider only vertices of secondary users, several of which are already blocked. Let us somewhat force notation and consider again that time $t = 0$ refers to the beginning of the secondary sensing phase. We thus have that $\mathscr{A}_0^S = \emptyset$, but the other two sets ($\mathscr{B}_0^S$ and $\mathscr{E}_0^S$) are actually the result of the primary sensing phase described before.

3.3. Markov Process and Fluid Limit

Note that in the configuration model described above, the process given by $(\mathscr{A}_t^P, \mathscr{B}_t^P, \mathscr{E}_t^P, \mathscr{B}_t^S, \mathscr{E}_t^S)$ constitutes a continuous-time Markov Process during the primary sensing phase, and analogously the process given by $(\mathscr{A}_t^S, \mathscr{B}_t^S, \mathscr{E}_t^S)$ constitutes a Markov Process during the secondary sensing phase. For instance, the time between transitions during the primary sensing phase is exponentially distributed with mean equal to $1/|\mathscr{E}_t^P|$ (since only unexplored nodes may become active at any given time).

However, since we are interested in the number of active nodes resulting from the sensing phases, our goal is to calculate $|\mathscr{A}_\infty^S|$, and not precisely which nodes are active. We thus follow the ideas presented in [8] and particularly [10], which chooses a set of variables that not only conforms a Markov Process, but is also amenable to a relatively simple analysis, in particular when the number of nodes tends to infinity.

Let us then define the following important variables:

- $E_t^P(i,j)$ and $E_t^S(i,j)$: number of unexplored primary and secondary nodes of degree (i,j) at time t.
- U_t^{PP}: number of unpaired half-edges at time t belonging to primary nodes and that should be connected to another primary node.
- U_t^{SS}: same as above but between secondary nodes.
- U_t^{PS}: number of unpaired half-edges at time t that belong to a primary node and should be connected to a secondary node or viceversa.[1]
- A_t^P and A_t^S: number of active primary and secondary nodes at time t

Initially we have the following conditions:

- all the vertices are unexplored: $E_0^P(i,j) = \mu(i,j)$ and $E_0^S(i,j) = \nu(i,j)$,
- all the half-edges are unpaired: $U_0^{PP} = \sum_{i,j} i\mu(i,j)$, $U_0^{PS} = \sum_{i,j} 2j\mu(i,j) = \sum_{i,j} 2i\nu(i,j) = \sum_{i,j} j\mu(i,j) + \sum_{i,j} i\nu(i,j)$ and $U_0^{SS} = \sum_i \sum_j j\nu(i,j)$,
- no transmitter is active: $A_0^P = A_0^S = 0$.

As we discuss below, during the primary sensing phase the process $X_t = (A_t^P, (E_t^P(i,j))_{i,j}, (E_t^S(i,j))_{i,j}, U_t^{PP}, U_t^{PS})$ also constitutes a continuous-time Markov Process. An analogous process will be defined for the secondary phase. Its Markovian structure allows us to analyze its asymptotic behavior by means of a simpler deterministic approximation. In a nutshell, we can say that by choosing a convenient scaling of the process it is possible to obtain in the limit, a description of the asymptotic behavior of the process as the solution of an ordinary differential equation system (hopefully deterministic) which is denominated "fluid limit". Whereas the stochastic process is a microscopic description of the system, the corresponding differential equation gives a macroscopic description that captures

[1] Please note that the number of unmatched half-edges that belong to a secondary node and that should be connected to a primary node is at all time equal to $U_t^{PS}/2$.

the main characteristics of the system. See for instance, classical results on convergence of Markov processes in [16] or [13]. The proof of this approximation result is generally based on a semi-martingale decomposition of the Markov process, which shows that the main characteristic of the stochastic process are captured by the drift part while the stochastic fluctuation of second order (corresponding to the martingale) vanishes with the scaling and limit procedure.

More specifically, consider a Markov process $X^N(t)$ parametric in N and its martingale decomposition:

$$X^N(t) = X^N(0) + \int_0^t Q_N(X^N(s))ds + M^N(t), \quad (1)$$

where $Q(l)$ is the so-called drift of the process at state l which may be calculated as $\sum_m (l-m)q(l,m)$, being $q(l,m)$ the transition rate from state l to m and $M^N(t)$ is a Martingale. Consider now the scaled process $\tilde{X}^N(t) = \frac{X^N(t)}{N}$, then:

$$\tilde{X}^N(t) = \tilde{X}^N(0) + \frac{1}{N}\int_0^t Q_N(X^N(s))ds + \frac{M^N(t)}{N}. \quad (2)$$

If there exist a Lipscthitz function Q such that

$$\lim_{N\to\infty} || \frac{Q_N(X^N(s))}{N} - Q(\tilde{X}^N(t)) || = 0$$

and $\frac{M^N(t)}{N}$ converges to zero in probability, then $\tilde{X}^N(t)$ converges in probability over compact time intervals to a deterministic process $x(t)$, described by the ODE (ordinary differential equation):

$$x'(t) = Q(x(t)). \quad (3)$$

The drift Q may be interpreted as the expected rate of change of the process. Even if the resulting deterministic differential equation is in many cases an intuitive description of the system, the proof of this kind of convergence or the process X_t is quite technical. The main issue in this case is that the process X_t is a measured-valued Markov process [14], which implies a careful definition of the topologies involved in the convergence result. Examples of formal proofs of convergence for this kind of processes in similar contexts can be found in [7, 8, 10]. In the next section we focus on the calculus of the drift for our process of interest X_t^N in order to determine the fluid limit (Theorem 1). Moreover, in this case we can obtain an explicit expression of $x(t)$ (solution of Eq. (3)).

3.3.1. Primary Sensing Phase

In this section we discuss the Markov structure of the process $X_t = X^{N_P}(t) = (A_t^P, (E_t^P(i,j))_{i,j}, (E_t^S(i,j))_{i,j}, U_t^{PP}, U_t^{PS})$ during the primary sensing phase and we calculate its drift. As we mentioned before, the drift determines the fluid limit. First of all, the times between transitions are exponentially distributed with mean $1/\sum_{i,j} E_t^P(i,j)$, since only primary unexplored nodes are competing for the channel (the rest are either blocked or already active). Let us then consider that at time t a primary node starts transmitting, and thus a transition occurs. Then the transition probabilities may be calculated as follows:

- A random node is uniformly chosen among all unexplored nodes and becomes active. Thus A_t^P increases by one with probability 1.
- The newly active node's degree distribution is simply:

$$\alpha_t(i,j) = \frac{E_t^P(i,j)}{\sum_{k,l} E_t^P(k,l)}.$$

  Suppose that the new transmitter has degree (I,J). This implies that it has I half-edges to be paired with other I unmatched half-edges (belonging to primary nodes), and J half-edges to be paired with other J ones (from secondary nodes). Then the number of unpaired half-edges U_t^{PP} and U_t^{SP} will be reduced by $2I$ and $2J$ respectively[2] with probability $\alpha_t(I,J)$.
- Let us focus on the neighbors of the tagged node, which should now be blocked. Assume we have to pair an unmatched half-edge to a primary node (one of the I half-edges from before). The pairing half-edge may be chosen from all those available (U_t^{PP}), of which precisely $iE_t(i,j)$ belong to an unexplored node with degree (i,j). Thus, the probability that any of the I primary neighbors of the tagged node is unexplored and has a degree (i,j) is equal to:

$$\beta_t^P(i,j) = \frac{iE_t^P(i,j)}{U_t^{PP}}.$$

  By a similar argument, the probability that any of the J secondary neighbors of the tagged node has a degree (i,j) and is unexplored is equal to:

$$\beta_t^S(i,j) = \frac{iE_t^S(i,j)}{U_t^{PS}/2}.$$

With the discussion above we are in conditions of calculating the drift of the process. For instance, A_t^P has a drift equal to $1 \times \sum_{i,j} E_t^P(i,j)$. Let us then normalize our process by the number of primary and secondary nodes N_P and N_S (where we will assume that N_P/N_S is a constant) and obtain a result such as Eq. (3).

Theorem 1. *Consider the configuration model discussed in Sec. 3.2 and the processes defined in Sec. 3.3 during the primary phase. Let us define the normalized processes, for which N_P/N_S is a constant:*

- $\tilde{A}_t^P = A_t^P/N_P$
- $\tilde{E}_t^P(i,j) = E_t^P(i,j)/N_P$ *and* $\tilde{E}_t^S(i,j) = E_t^S(i,j)/N_S$

[2] Please note that the existence of loops or multi-edges are possible with the configuration model discussed in Sec. 3.2. For instance, actually U_t^{PP} should be decreased by $2I-2L$ (with L the number of self-loops). However, as indicated by intuition, proved in [8, 10], and further discussed in [7], when the number of nodes goes to infinity, as we will consider next, the probability of such occurrences may be neglected in the analysis.

- $\tilde{U}_t^{PP} = U_t^{PP}/N_P$ *and* $\tilde{U}_t^{SP} = U_t^{SP}/N_P$

Let be $\tilde{X}_t^N = (\tilde{A}_t^P, \tilde{E}_t^P(i,j), \tilde{E}_t^S(i,j), \tilde{U}_t^{PP}, \tilde{U}_t^{SP})$. *Therefore, as* $N_P \to \infty$, $\tilde{X}_t^N$ *converges in probability over compact time intervals to* $x^P(t) = (a_t^P, e_t^P(i,j), e_t^S(i,j), u_t^{PP}, u_t^{PS})$ *solution of the following differential equation system:*

$$\frac{da_t^P}{dt} = \sum_{k,l\in\mathbb{N}} e_t^P(k,l); \tag{4}$$

$$\frac{de_t^P(i,j)}{dt} = -e_t^P(i,j) - \frac{ie_t^P(i,j)}{u_t^{PP}} \sum_{k,l\in\mathbb{N}} ke_t^P(k,l);\ \forall i,j\in\mathbb{N}; \tag{5}$$

$$\frac{de_t^S(i,j)}{dt} = -\frac{2ie_t^S(i,j)}{u_t^{PS}} \sum_{k,l\in\mathbb{N}} le_t^P(k,l);\ \forall i,j\in\mathbb{N}; \tag{6}$$

$$\frac{du_t^{PP}}{dt} = -2\sum_{k,l\in\mathbb{N}} ke_t^P(k,l); \tag{7}$$

$$\frac{du_t^{PS}}{dt} = -2\sum_{k,l\in\mathbb{N}} le_t^P(k,l); \tag{8}$$

where

$$a_0^P = 0;$$

$$e_0^P(i,j) = \frac{\mu(i,j)}{N_P};\ \forall i,j\in\mathbb{N}\ \textit{and}\ e_0^S(i,j) = \frac{\nu(i,j)}{N_s};\ \forall i,j\in\mathbb{N};$$

$$u_0^{PP} = \frac{1}{N_P}\sum_{i=0}^{\infty}\sum_{i=0}^{\infty} i\mu(i,j)\ \textit{and}\ u_0^{PS} = \frac{1}{N_P}\sum_{i=0}^{\infty}\sum_{i=0}^{\infty} 2j\mu(i,j).$$

Some remarks are in order concerning the result above. Firstly, the original Markov Chain has an absorbing state for which $E_t^P(i,j) = 0\,\forall i,j$. This is reflected in the set of equations above, where we have an equilibrium point when $e_t^P(i,j) = 0\,\forall i,j$.

Secondly, and as we mentioned before, primary nodes act independently of secondary ones. This is again reflected in the set of equations, where the key is to solve equations (5) and (7) which are coupled (the rest may be solved once we obtain an analytical expression for $e_t^P(i,j)$, see details in Appendix A), and refer to the behavior of these nodes.

Thirdly, we can include into our model unsaturated traffic conditions for primary users. We model this aspect by incorporating the transmission probability p_{PU}. This parameter defines the number of primary transmitters that have packets to be sent in each time slot. In other words, in this phase of the algorithm only the primary unexplored nodes which have packet to be sent are competing for the channel. This only affects $e_0^P(i,j)$ value as $e_0^P(i,j) = p_{PU}\frac{\mu(i,j)}{N_P};\ \forall i,j\in\mathbb{N}$.

Lastly, we are actually interested in how many secondary nodes are still unexplored after the primary sensing phase is over, so as to study the secondary phase. That is to say, we want to calculate $e_\infty^S(i,j)\ \forall i,j$, which will in turn become the initial conditions of the secondary sensing phase. This value may be calculated as follows:

Theorem 2. *Consider the processes and variables defined in Theorem 1. Let* τ_∞ *be the unique value in* $(0,\infty]$ *such that*

$$\int_0^{\tau_\infty} \frac{u_0^{PP}e^{-2\sigma}}{\sum_{k,l\in\mathbb{N}} ke_0^P(k,l)e^{-k\sigma}}d\sigma = 1. \tag{9}$$

Then, the proportion of unexplored secondary nodes at the beginning of the secondary phase converges in probability to:

$$e_\infty^S(i,j) = e_0^S(i,j)\left(\frac{u_{\tau_\infty}^{PS}}{u_0^{PS}}\right)^i \forall(i,j), \tag{10}$$

where

$$u_{\tau_\infty}^{PS} = u_0^{PS} - 2\int_0^{\tau_\infty}\sum_{k,l\in\mathbb{N}} le_0^P(k,l)e^{-k\sigma}\frac{u_0^{PP}e^{-2\sigma}}{\sum_{k,l\in\mathbb{N}} ke_0^P(k,l)e^{-k\sigma}}d\sigma. \tag{11}$$

Proof. See the appendix. □

Some interesting insights may be obtained from the result of equation (10). For instance, and as we mentioned before, the result of the primary phase is not influenced by the secondary nodes. This is reflected by the fact that the proportion of secondary nodes that are still unexplored after the primary sensing phase only depends on the degree towards primary nodes (the variable i). More in particular, its form is exponential on i, generating great differences between secondary nodes regarding their access probability. Since $u_{\tau_\infty}^{PS}/u_0^{PS} < 1$, those who belong to the protection zone of several primary nodes will seldomly access the channel.

Please note that $u_{\tau_\infty}^{PS}/u_0^{PS}$ represents the proportion of unpaired half-edges between primary and secondary users at the end of the primary sensing phase. These unpaired half edges correspond to primary users that did not become active. Therefore, the quotient may be interpreted as the probability of a secondary user to be out of the protection zones of active primary nodes.

3.3.2. Secondary Sensing Phase

Once the primary sensing phase is over, we turn our attention to the secondary sensing phase. The construction of the Markov Process will be very similar to the previous sections, but in this case is a little simpler, since we do not have to take into account primary nodes. In this sense, let us somewhat abuse the notation and define $E_t^S(j)$ as the number of unexplored secondary nodes during the secondary sensing phase that have j half-edges to be paired with other secondary nodes. Then, the initial condition $E_0^S(j)$ is the result of the primary sensing phase, and will be estimated from $e_\infty^S(k,j)$ as defined in (10). It should be noted that the existence of the limit $\lim_{t\to\infty} e_t^S(k,j)$ (stationary regime) should be guaranteed. The existence of this limit is related to the ergodicity of the process and it can be proved with similar arguments to the ones included in [4] and the references therein.

Finally, with arguments very similar to the ones used in the previous subsection, we reach the following result:

Theorem 3. *Consider the configuration model discussed in Sec. 3.2, $E_t^S(j)$ as defined above, and the processes defined in Sec. 3.3 during the secondary sensing phase. Furthermore, let $e_\infty^S(i,j)$ be the value defined in* (10)*. Let us define the normalized processes $\tilde{A}_t^S = A_t^S/N_S$, $\tilde{E}_t^S(j) = E_t^S(j)/N_S$, and $\tilde{U}_t^{SS} = U_t^{SS}/N_S$.*

Then, as $N_S \to \infty$, they converge in probability to the solution of the following set of differential equations:

$$\frac{da_t^S}{dt} = \sum_{l\in\mathbb{N}} e_t^S(l); \tag{12}$$

$$\frac{de_t^S(j)}{dt} = -e_t^S(j) - \frac{je_t^S(j)}{u_t^{SS}} \sum_{l\in\mathbb{N}} le_t^S(l);\ \forall j \in \mathbb{N}; \tag{13}$$

$$\frac{du_t^{SS}}{dt} = -2\sum_{l\in\mathbb{N}} le_t^S(l); \tag{14}$$

where

$$a_0^S = 0;$$
$$e_0^S(j) = \sum_{k\in\mathbb{N}} e_\infty^S(k,j)\ \forall j \in \mathbb{N}$$
$$u_0^{SS} = \frac{1}{N_S}\sum_{l\in\mathbb{N}} l\nu(k,l);$$

Again, we are interested only on the limit of a_t^S as t goes to infinity (when the secondary sensing phase is over). By similar manipulations of the differential equations (Eq. (12-14) can be resolved explicitly, see details in Appendix B) the following result may be obtained:

Theorem 4. *Consider the processes and variables defined in Theorem 3. Let τ_∞ be the unique value in $(0,\infty]$ such that*

$$\int_0^{\tau_\infty} \frac{u_0^{SS}e^{-2\sigma}}{\sum_{l\in\mathbb{N}} le_0^S(l)e^{-l\sigma}} d\sigma = 1. \tag{15}$$

Then, the proportion of active secondary transmitters converges in probability to:

$$a_\infty^S = \int_0^{\tau_\infty} \sum_{j\in\mathbb{N}} e_0^S(j)e^{-j\tau} \frac{u_0^{SS}e^{-2\tau}}{\sum_{j\in\mathbb{N}} je_0^S(j)e^{-j\tau}} d\tau \tag{16}$$

Proof. See the appendix. □

Analogously, it is possible to demonstrate that the proportion of active secondary transmitters of degree j, converges in probability to:

$$a_\infty^S(j) = \int_0^{\tau_\infty} e_0^S(j)e^{-j\tau} \frac{u_0^{SS}e^{-2\tau}}{\sum_{k\in\mathbb{N}} ke_0^S(k)e^{-k\tau}} d\tau, \forall j. \tag{17}$$

In this phase of the algorithm, the Markov Chain has an absorbing state where $E_t^S(j) = 0 \forall j$ (it finishes when all secondary nodes are active or blocked). This is reflected in the set of equations above, where we have an equilibrium point when $e_t^S(j) = 0 \forall j$. In addition, in Eq. (17) we can observe that the medium access probability is influenced by the node's degrees. This is reasonable because the larger j is, the larger the probability of being blocked by another secondary node is.

4. Simulated Experiments and Results

In order to validate the proposed approximation we will present an example considering a large but finite number of nodes. We calculate the MAP_{SU} using our deterministic expression (Eq. (16)) and we compare it with the results obtained of several simulations of the stochastic process $\tilde{A}_\infty^S$. We also show the accuracy of our methodology analyzing several realizations of the process $\tilde{E}_t^S(i,j)$ with its associated deterministic estimation $e_t^S(i,j)$ in both phases of the algorithm. In the next section we compare our results with results for spatial models based on stochastic geometry techniques. Finally, we complete our validation by testing the methodology in other representative scenarios.

Before introducing the particular example, let us now explain the validation method. First we simulate a graph that satisfies certain characteristics (the characteristics are defined according to the network we want to simulate). Given the graph, we can extract the counting measures $\mu(i,j)$ and $\nu(i,j)$ and then we apply the results of Theorems 1, 2, 3 and 4 obtaining deterministic approximations of several metrics, in particular the estimation of the MAP_{SU}. On the other hand, having the graph we proceed to simulate several realizations of the stochastic process (its evolution is related with the considered MAC protocol) and as a result we obtain the simulated metrics of interest.

In this section, as a first illustration of the accuracy of our proposal, we choose the variation of the Erdös-Rényi model that was described in Sec. 3.1. In particular we consider $k = 1\ldots10$, where $k = k_{PP} = k_{PS} = k_{SS}$. Consequently, for each k value, we have that on average, each PU has k primary neighbors and k secondary users in its protection zone. In addition, each SU has on average k secondary neighbors.

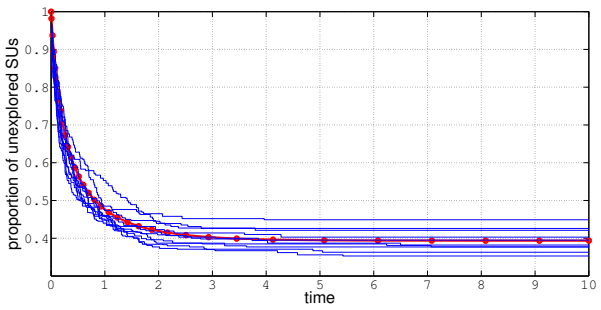

Figure 2: $\sum_i\sum_j \tilde{E}_t^S(i,j)$ during the Primary Sensing Phase. The deterministic estimation Eq. (6) is marked with circles. Parameters: $N_P = 500$, $N_S = 1000$, $p_{PU} = 0.5$ and $k = 10$.

Several realizations of $\sum_i\sum_j \tilde{E}_t^S(i,j)$, where the graphs have the characteristics explained before, are shown in Figures 2 and 3 along with the solutions of Eq. (6) and Eq. (13) respectively. As an example we show the performance of a specific k value ($k = 10$). Figure 2 represents the evolution of the proportion of unexplored SUs during the Primary Sensing Phase. We can observe that in Figure 3 (which represents the same but during the Secondary Sensing Phase) the initial condition coincides with the limit value in Figure 2. As expected, the limit value that

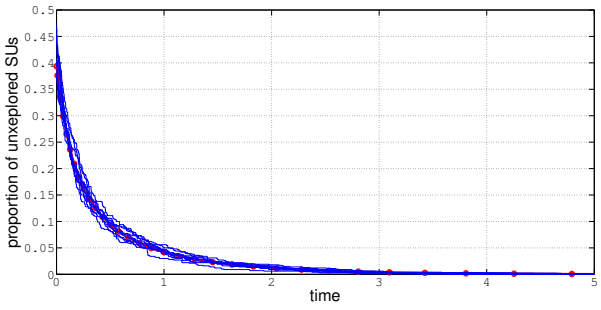

Figure 3: $\sum_i \sum_j \tilde{E}_t^S(i,j)$ during the Secondary Sensing Phase. The deterministic estimation Eq. (13) is marked with circles. Parameters: $N_P = 500$, $N_S = 1000$, $p_{PU} = 0.5$ and $k = 10$.

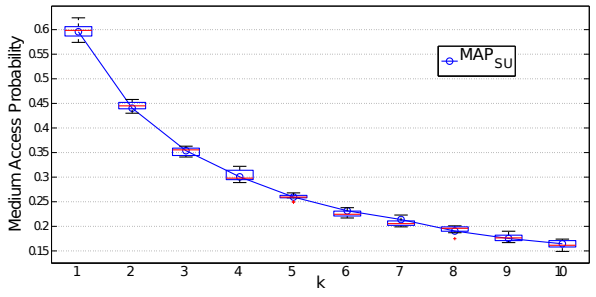

Figure 4: The evaluation of Eq. (16) along with the boxplot of the numerical results of 10 simulations with parameters: $N_P = 500$, $N_S = 1000$, $p_{PU} = 0.5$ and $k = 1 \ldots 10$.

is shown in Figure 3 is 0 (when the process finishes, no SU is unexplored). These figures illustrate how $e_t^S(i,j)$ effectively represents the mean of $\tilde{E}_t^S(i,j)$ in both phases of the algorithm. Similar results were obtained for the other involved stochastic processes.

Finally, in Figure 4 we show the performance of the methodology for the different values of the parameter k (k is located in the abscissa). The larger k is, the larger the connection probabilities are and then, the smaller the medium access probability of SUs is. We can conclude that Eq. (16) provides an accurate approximation of the access medium probability.

5. Comparison with spatial models

In this section we compare our proposal with a result based on stochastic geometry and point processes. This type of analysis focuses on the random spatial location of users and aim at estimating the medium access probability (and other metrics) for a given user configuration. We have chosen to compare the results of the article [21] which have been extended in [22]. In these articles, the authors proposed a probabilistic model to analyze the cognitive radio paradigm in large wireless networks with randomly located users. The authors also used Cognitive-CSMA as the medium access mechanism.

This section is organized as follows. First, we introduce the probabilistic model of [21, 22] and their analytical results. We also propose a modification in their model in order to be in a "comparable" context to ours. Finally we present two representative examples to compare both results.

5.1. An approximation of the medium access probability using a stochastic geometry analysis

Using a stochastic geometry approach, the location of the nodes of the network is seen as the realization of one or many point processes. This means that the network can be considered as a snapshot of a stationary random model in the (Euclidean) space which is possible to analyze in a probabilistic way. The time is divided into slots and one slot is needed to transmit a packet for all users. Then, one snapshot represents the nodes spatial distribution in one time slot.

In the articles [21, 22] the users of the network are assumed to be a realization of two independent marked Poisson point processes (PPP) $\Phi_p = \{X_i^p, t_i^p\}$ and $\Phi_s = \{X_i^s, t_i^s\}$ with intensities λ_p and λ_s on $\mathbb{R}^2$ respectively. $\{X_i^p\}$ and $\{X_i^s\}$ denotes the positions of the potential primary and secondary transmitters, and t_i^p (and t_i^s) models the backoff timers used in the Cognitive-CSMA protocol ($\{t_i^p\}$ and $\{t_i^s\}$ are i.i.d r.vs. uniformly distributed in $[0,1]$). The model also features an infinite symmetric matrix $F = \{F(i,j)_{i,j}\}$ which models the fading of the channel from user i to user j (being i and j two arbitrary transmitters, PU or SU). A deterministic attenuation $\alpha > 2$ is also assumed (i.e. $L(d) = d^{-\alpha}$, being d the distance between two nodes). Considering those features we can say that the power received from i by j is:

$$P(i,j) = P(i)F(i,j)L(\|X_j - X_i\|). \tag{18}$$

With that in mind, conforming to the medium access mechanism, a primary transmitter will access to the channel if it has the smallest timer among its primary contenders. For secondary transmitters, it will access if it has no active primary contender and it has the smallest timer between its secondary neighbors. Then, for each primary node $i \in \Phi_p$ we can define the set of its primary neighbors ($\mathcal{N}_i^p$) as

$$\mathcal{N}_i^p = \{j \in \Phi_p : \frac{F(j,i)}{\|X_i^p - X_j^p\|^\alpha} > \rho, j \neq i\}, \tag{19}$$

where ρ is a threshold that determines how sensitive the CS is. Please note that in this model, $P(j)$ is assumed constant and included in $F(j,i)$ which is considered as a virtual power.

On the other hand, for each secondary user $i \in \Phi_s$, we need to know the sets of: its active primary contenders ($\mathcal{N}'^p_i$) and its secondary contenders ($\mathcal{N}'^s_i$). Letting Φ_p^* be the process of active primary transmitters, these sets can be defined as

$$\mathcal{N}'^p_i = \{j \in \Phi_p^* : \frac{F(j,i)}{\|X_i^s - X_j^p\|^\alpha} > \rho'\} \text{ and} \tag{20}$$

$$\mathcal{N}'^s_i = \{j \in \Phi_s : \frac{F(j,i)}{\|X_i^s - X_j^s\|^\alpha} > \rho', j \neq i\} \tag{21}$$

respectively.

According to that, the primary and secondary retain indicators are:

$$R_i^p = \mathbb{1}_{\{t_i^p < t_j^p \, \forall X_j^p \in \mathcal{N}_i^p\}} \text{ and} \tag{22}$$

$$R_i^s = \mathbb{1}_{\{t_i^s < t_j^s \, \forall X_j^s \in \mathcal{N}'^s_i, \, \mathbb{1}_{|\mathcal{N}'^p_j|=0}\}} \mathbb{1}_{\{|\mathcal{N}'^p_i|=0\}}. \tag{23}$$

This means that the medium access probabilities are $MAP_{PU} = P(R_i^p = 1)$ and $MAP_{SU} = P(R_i^s = 1)$. The first term of Eq. (23) corresponds to the case where the timer of the secondary transmitter i is smaller than all the timers of its secondary neighbors ($t_i^s < t_j^s \; \forall X_j^s \in \mathcal{N}'^s_i$) considering only the ones which are not in a primary protection zone of an active PU ($\mathbb{1}_{|\mathcal{N}'^p_j|=0}$). The second term says that the secondary transmitter i is not in a primary protection zone of an active PU ($\mathbb{1}_{|\mathcal{N}'^p_i|=0}$).

The authors of [21, 22] obtain a conservative approximation of MAP_{SU}. They simplified the model considering that a SU will be preempted if it has one or more primary contenders no matter whether the contenders are active or not. Therefore, many secondary users, which are in conditions to use the band, might be silenced. In this context, the MAP probability expressions for PUs and SUs are:

$$MAP_{PU} = \frac{1 - e^{-\lambda_p \bar{N}_0}}{\lambda_p \bar{N}_0} \text{ and} \tag{24}$$

$$MAP_{SU} \approx \frac{1 - e^{-\lambda_s \bar{N}_0 e^{-\lambda_p \bar{N}_0}}}{\lambda_s \bar{N}_0}, \tag{25}$$

where $\bar{N}_0$ is the mean number of contenders of a typical user in a network of intensity 1 and $G(t) = P(F \leq t)$ is the fading c.d.f.:

$$\bar{N}_0 = \int_{\mathbb{R}^2} (1 - G(\rho |x|^\alpha)) dx. \tag{26}$$

Without loss of generality, we have considered $\rho = \rho'$.

The calculus for secondary users MAP is approximated because the authors of [21, 22] considered the non preempted secondary users as an independent thinned process from secondary users process with thinning probability $e^{-\lambda_p \bar{N}_0}$. For more details see [21].

Complementing the articles [21, 22] we propose an improvement in the estimation of Eq. (25). The idea is to apply an analogous assumption of [21] in order to model the active PU process Φ_p^* as a PPP. Taking this into account, the idea is to approximate the process Φ_p^* by an independent thinning of PU process Φ_p with thinning probability MAP_{PU}. In this context, we can apply the retain indicator defined by Eq. (23) obtaining a non conservative estimation of the MAP_{SU} and also more appropriate to compare to our results:

$$MAP_{SU} \approx \frac{1 - e^{-\lambda_s \bar{N}_0 e^{-\lambda_p MAP_{PU} \bar{N}_0}}}{\lambda_s \bar{N}_0}. \tag{27}$$

Please note that the fading variables are assumed to be independent of the nodes positions.

5.2. Numerical examples

In this section we choose three representative examples in order to illustrate the accuracy and the applicability of both approximations (our estimation using random graphs Eq. (16) and the one presented in Eq. (27)). In particular, in all cases we have assumed a Rayleigh fading ($G(t) = 1 - e^{-\theta t}$) because in this situation $\bar{N}_0$ has a closed formula to be used in Eq. (27):

$$\bar{N}_0 = \frac{2\pi \Gamma(2/\alpha)}{\alpha (\rho \theta)^{2/\alpha}}, \tag{28}$$

where $\Gamma(.)$ is the Euler Gamma function.

We consider different values of fading mean θ. For each θ value, we run several independent simulations of the access process. In order to evaluate the performance of both approaches, we consider as the true MAP the one provided by the average of all the simulations.

5.2.1. Example 1: Poisson Point Processes

In this particular case, given a realization of two spatial PPPs (Φ_p and Φ_s with intensities λ_p and λ_s) and the fading variables between any pair of nodes, the conflict graph is built considering also the path-loss phenomenon according to the definitions of $\mathcal{N}_i^p$, $\mathcal{N}'^p_i$ and $\mathcal{N}'^s_i$. Once the graph is obtained, we extract the values of N_S, N_P and the measures $\mu(i,j)$ and $\nu(i,j)$, and we proceed in the same way as in Sec. 4.

For each θ value, we run 10 independent simulations and in Figure 5 we present the analytical results (of both estimations) together with the corresponding simulated values.

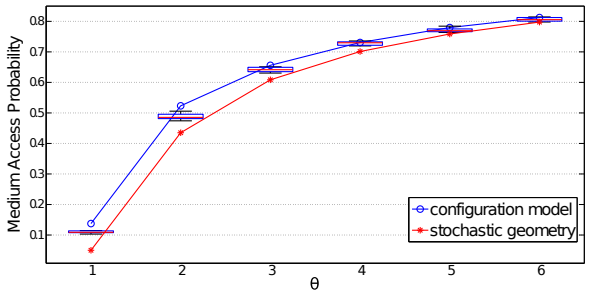

Figure 5: Evaluation of Eq. (16) and Eq. (27) along with the boxplot of the numerical results of 10 simulations with parameters: $\lambda_p = 1.6$ ($p_{PU} = 0.5$ and $\bar{N}_P = 500$), $\lambda_s = 6.4$ ($\bar{N}_S = 2000$), $\alpha = 3$, considering different values of θ.

Some remarks regarding the obtained results. Firstly, our random graph estimation of the MAP_{SU} shows a very good performance complementing the results of Sec. 4. Please note that our method considers a graph which is chosen randomly among all graphs that comply with the initial measures $\mu(i,j)$ and $\nu(i,j)$. This means, that in this example our configuration model ignores correlations that appear when spatial features are considered. This explains why the performance results in the Erdös-Rényi case (Figure 4) are better than in this case. Even more, this is the reason that justifies the improvement in the accuracy when θ is large. In other words, the effects of the ignored aspects decrease when the amount of noise in the graph increases.

Secondly, we observe that the stochastic geometry estimation has a good accuracy too. Eq. (27) was obtained assuming that active primary (and secondary) users are located according to a realization of an homogeneous PPP; consequently the larger θ is, the more reasonable this assumption is, and then, the more accurate the MAP approximation is.

Lastly, we can conclude that in this particular scenario both approaches are suitable despite considering a finite number of nodes.

5.2.2. *Example 2: Grid Configuration for Primary Users*

A natural scenario for cognitive radio networks, corresponds to a planned primary topology together with a disordered and random secondary one. Therefore, in this second example, we choose a particular fixed configuration for the primary nodes. We consider that PUs are located in a perfect grid configuration and SUs are located according to a realization of a PPP (see for instance Figure 6). Please note that this PUs configuration is not in the hypothesis of none of the analyzed methods. In particular, the communication graph is not totally random since the nodes are located in a specific configuration. Despite of this fact, we are going to test how versatile the two approaches are.

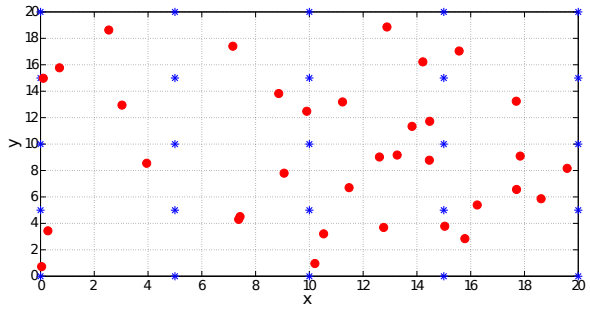

Figure 6: Example of a primary grid configuration (stars) with random secondary nodes (circles).

We apply Eq. (27) as if the primary process was a PPP. In this case, in order to apply the stochastic geometry expressions, the natural thing to do is to estimate the process intensities. Then, the primary intensity can be calculated as $\lambda_p = \frac{N_P}{L^2}$ where L is the dimension of the grid. For instance, in the example scenario of Figure 6 we can say that $\lambda_p = \frac{25}{20^2}$.

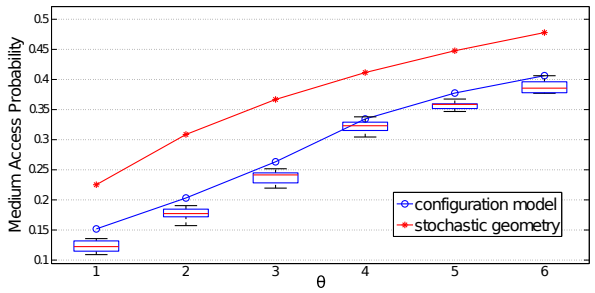

Figure 7: Evaluation of Eq. (16) and Eq. (27) along with the boxplot of the numerical results of 10 simulations with parameters: $\lambda_p = 0.005$ ($p_{PU} = 1$), $\lambda_s = 0.007$, $\alpha = 3$, $L = 360$, considering different values of θ.

In Figure 7 we show the performance of both approaches together with the simulated results. The obtained result reflects a poor performance of the spatial model while our random graph approximation shows a better performance. This represents a limitation of the spatial model's application, more specifically when the involved point processes are not all Poisson. In addition, in this case is more evident the fact that our proposed approximation ignores spatial correlation (see Figures 4 and 5 and compare them with Figure 7). Primary users are located in a specific fixed configuration but thanks to the randomness provided by the fading, the resulting performance indicators still give excellent approximations.

It is important to remark that, if the fading variables were constant, the approximations of Eq. (25) and Eq. (27) would lack of sense. In addition, in many cases determining closed analytical expression of performance metrics using stochastic geometry techniques represents a difficult task.

5.2.3. *Example 3: Real configurations for Primary Users*

We conduct two more realistic experiments to evaluate secondary MAP where locations of PUs are provided by the open source project OpenCellID [1]. This project maintains a complete and open database from which we can easily retrieve latitude and longitude information of the cell-towers of a target geographic area.

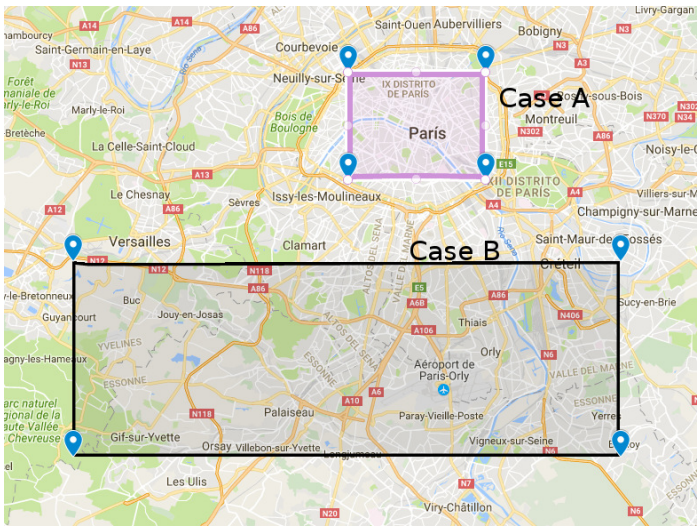

Figure 8: Geographical zones chosen for real scenarios: Case A and B. Case A is located in the heart of Paris and Case B in its suburbs.

We consider two different scenarios (see Figure 8), one with a high density of users (Case A: center of Paris) and another with a medium density (Case B: Paris suburbs). In both cases PUs are deployed according to data from cell-tower locations of one LTE-operator and SUs are deployed following a PPP. Figures 9 and 10 show the PU spatial distributions; please note that Case A has approximately twice the user intensity of Case B.

Given the two point process (Φ_p and Φ_s with intensities λ_p and λ_s) and the fading variables between any pair of nodes, the conflict graph (nodes which are neighbors to each other) is built considering also the path-loss phenomenon according to the definitions of $\mathcal{N}_i^p$, $\mathcal{N}'^p_i$ and $\mathcal{N}'^s_i$. We consider different values of fading mean θ, and for each θ the measures $\mu(i,j)$ and $\nu(i,j)$ are obtained. As in Example 2 we apply Eq. (27) as if the primary processes were distributed as PPPs.

In Figures 11 and 12 we show the performance of both approaches together with the simulation results. Some remarks are in order concerning the obtained results. Firstly, our estimation of the MAP_{SU} shows an excellent performance in both

Figure 9: Case A: Points represent 2412 primary users located in an area of $47km^2$.

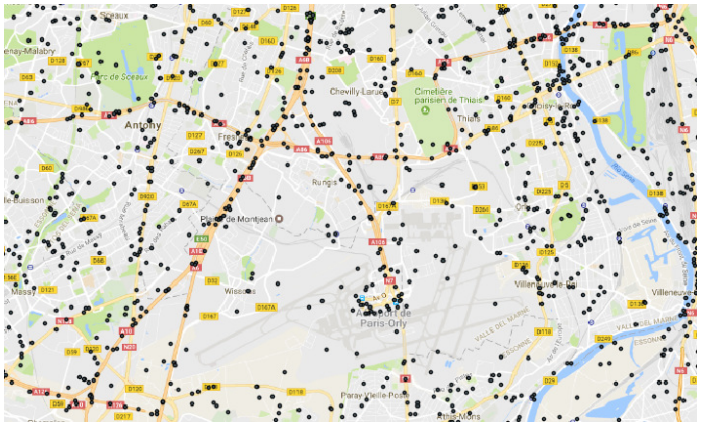

Figure 10: Case B: Points represent primary users (for the sake of presentation we show a specific zoom area). Scenario B considers a total of 1996 primary users located in an area of $83km^2$.

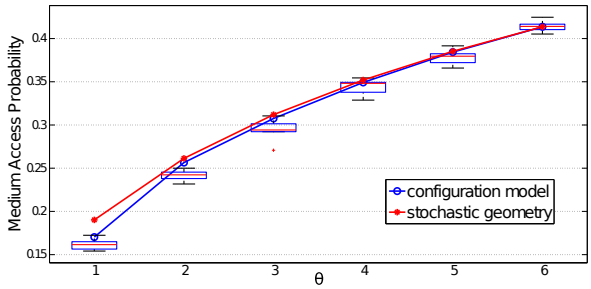

Figure 11: Case A performance results. Simulation Parameters: $N_P = 2412$, $N_S = 1800$, $p_{PU} = 0.4$, $\alpha = 3$, considering different values of θ.

cases. This demonstrates the versatility of our technique. We can also see the improvement in the accuracy when θ increases, due to the spatial correlation becoming weaker. Secondly, we observe that the stochastic geometry estimation has a good accuracy in Case A but a poor performance in Case B. The bad

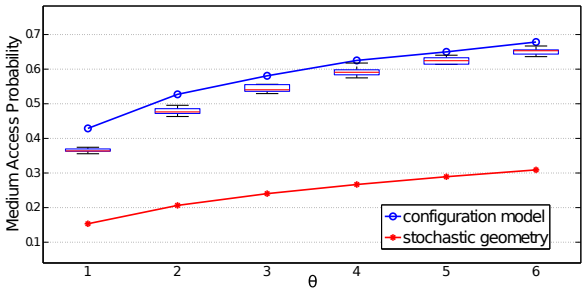

Figure 12: Case B performance results. Simulation Parameters: $N_P = 1996$, $N_S = 1237$, $p_{PU} = 0.6$, $\alpha = 3$, considering different values of θ.

performance can be explained by non-homogeneous and non-Poisson characteristics of Φ_p: in Case B there are large areas without the presence of PUs and it also presents some clusters (see for example the airport zone). Maybe the stochastic geometry performance could be improved in this scenario if Φ_p is represented by a Poisson Cluster Process [12, 3], but this model is out of the scope of the present paper.

6. Conclusions and Future Work

We extended the methodology developed in [8] in the particular case of a cognitive radio network. With our proposal, we showed that it is possible to calculate an analytic approximation of the medium access probability (both for PUs and, most importantly, SUs) in an arbitrary large heterogeneous random network. This performance metric gives an idea of the possibilities offered by cognitive radio to improve the spectrum utilization.

Through extensive simulations, including real scenarios of primary network deployments, we have verified that the approximation obtained is accurate. We have also illustrated a performance comparison between our estimation and the one obtained by a stochastic geometry approach. As a future line, we want to characterize which scenarios are more suitable for the application of our estimation and which are not.

Another interesting future research line is the study of the degradation of PU's communications caused by the presence of SUs. In other words, the question to be answered is: how many transmission fail in mean? This is strongly related with the channel model characteristics. This analysis and its inclusion in a random graph model is a challenging task for a future work.

Acknowledgments

This work was financially supported by CSIC (Grupo I+D Artes and Proyecto I+D "Límites fluidos, aproximación por difusión y grandes desvíos en sistemas de comunicación de gran dimensión.") and a CAP-UdelaR scholarship.

References

[1] Opencellid, [online], https://opencellid.org/.

[2] Cisco visual networking index: Global mobile data traffic forecast update, 2015–2020. white paper. Tech. rep., Cisco, Feb 2016.

[3] AFSHANG, M., AND DHILLON, H. S. Poisson cluster process based analysis of hetnets with correlated user and base station locations. *CoRR abs/1612.07285* (2016).

[4] ASPIROT, L., MORDECKI, E., AND RUBINO, G. Fluid limits applied to peer to peer network analysis. *Quantitative Evaluation of Systems, International Conference on 0* (2011), 13–20.

[5] BACCELLI, F., AND BLASZCZYSZYN, B. *Stochastic Geometry and Wireless Networks, Volume I - Theory*, vol. 1 of *Foundations and Trends in Networking Vol. 3: No 3-4, pp 249-449*. NoW Publishers, 2009.

[6] BACCELLI, F., AND BLASZCZYSZYN, B. *Stochastic Geometry and Wireless Networks, Volume II - Applications*, vol. 2 of *Foundations and Trends in Networking: Vol. 4: No 1-2, pp 1-312*. NoW Publishers, 2009.

[7] BERMOLEN, P., JONCKHEERE, M., LARROCA, F., AND MOYAL, P. Estimating the transmission probability in wireless networks with configuration models. *ACM Trans. Model. Perform. Eval. Comput. Syst. 1*, 2 (Apr. 2016), 9:1–9:23.

[8] BERMOLEN, P., JONCKHEERE, M., AND MOYAL, P. The jamming constant of uniform random graphs. *Stochastic Processes and their Applications* (2016). To appear.

[9] BOLLOBAS, B. *Random Graphs*. Cambridge University Press, Cambridge, UK, 2001.

[10] BRIGHTWELL, G., JANSON, S., AND LUCZAK, M. The greedy independent set in a random graph with given degrees. *Random Structures Algorithms,* (Oct. 2016). To appear.

[11] CAPDEHOURAT, G., LARROCA, F., AND BELZARENA, P. Decentralized robust spectrum allocation for cognitive radio wireless mesh networks. *Ad Hoc Networks 36, Part 1* (2016), 1 – 20.

[12] CHUN, Y. J., HASNA, M. O., AND GHRAYEB, A. Modeling heterogeneous cellular networks interference using poisson cluster processes. *IEEE Journal on Selected Areas in Communications 33*, 10 (Oct 2015), 2182–2195.

[13] DARLING, R., AND NORRIS, J. Differential equation approximations for markov chains. *Probab. Surveys 5* (2008), 37–79.

[14] DAWSON, D. Measure-valued processes, stochastic partial differential equations, and interacting systems. In *CRM Proceedings & Lecture Notes* (1991), vol. 5, American Mathematical Society.

[15] ERDŐS, P., AND RÉNYI, A. On random graphs. I. *Publ. Math. Debrecen 6* (1959), 290–297.

[16] ETHIER, S. N., AND KURTZ, T. G. *Markov processes : characterization and convergence*. Wiley series in probability and mathematical statistics. J. Wiley & Sons, New York, Chichester, 1986.

[17] HAENGGI, M., ANDREWS, J. G., BACCELLI, F., DOUSSE, O., AND FRANCESCHETTI, M. Stochastic geometry and random graphs for the analysis and design of wireless networks. *IEEE Journal on Selected Areas in Communications 27*, 7 (September 2009), 1029–1046.

[18] LEE, S., AND HWANG, G. *Throughput Analysis of Multichannel Cognitive Radio Networks Based on Stochastic Geometry*. Springer International Publishing, Cham, 2016, pp. 63–71.

[19] MITOLA, J., AND MAGUIRE, G. Q. Cognitive radio: making software radios more personal. *IEEE Personal Communications 6*, 4 (Aug 1999), 13–18.

[20] MOLLOY, M., AND REED, B. A critical point for random graphs with a given degree sequence. *Random Structures & Algorithms 6*, 2-3 (1995), 161–180.

[21] NGUYEN, T. V., AND BACCELLI, F. A probabilistic model of carrier sensing based cognitive radio. In *New Frontiers in Dynamic Spectrum, 2010 IEEE Symposium on* (April 2010), pp. 1–12.

[22] NGUYEN, T. V., AND BACCELLI, F. A stochastic geometry model for cognitive radio networks. *The Computer Journal* (2011).

[23] PANAHI, F. H., AND OHTSUKI, T. Stochastic geometry based analytical modeling of cognitive heterogeneous cellular networks. In *2014 IEEE International Conference on Communications (ICC)* (June 2014), pp. 5281–5286.

[24] REN, J., ZHANG, Y., ZHANG, N., ZHANG, D., AND SHEN, X. Dynamic channel access to improve energy efficiency in cognitive radio sensor networks. *IEEE Transactions on Wireless Communications 15*, 5 (May 2016), 3143–3156.

[25] SHARMA, S. K., LAGUNAS, E., CHATZINOTAS, S., AND OTTERSTEN, B. Application of compressive sensing in cognitive radio communications: A survey. *IEEE Communications Surveys Tutorials 18*, 3 (thirdquarter 2016), 1838–1860.

[26] STOYAN, D., KENDALL, W. S., AND MECKE, J. *Stochastic geometry and its applications*. Wiley series in probability and mathematical statisitics. Wiley, Chichester, W. Sussex, New York, 1987. Rev. translation of: Stochastische Geometrie.

[27] TSIROPOULOS, G. I., DOBRE, O. A., AHMED, M. H., AND BADDOUR, K. E. Radio resource allocation techniques for efficient spectrum access in cognitive radio networks. *IEEE Communications Surveys Tutorials 18*, 1 (Firstquarter 2016), 824–847.

[28] VAN DER HOFSTAD, R. Random graphs and complex networks. Lecture Notes, 2013.

Appendix A. A Proof of Theorem 2

According to Theorem 1, we have defined, during the primary sensing phase, the normalized processes:

- $\tilde{A}_t^P = A_t^P/N_P$,
- $\tilde{E}_t^P(i,j) = E_t^P(i,j)/N_P$ and $\tilde{E}_t^S(i,j) = E_t^S(i,j)/N_S$,
- $\tilde{U}_t^{PP} = U_t^{PP}/N_P$ and $\tilde{U}_t^{SP} = U_t^{SP}/N_P$,

which converge in probability to $(a_t^P, e_t^P(i,j), e_t^S(i,j), u_t^{PP}, u_t^{PS})$ solution of the following differential equation system:

$$\frac{da_t^P}{dt} = \sum_{k,l\in\mathbb{N}} e_t^P(k,l); \tag{A.1}$$

$$\frac{de_t^P(i,j)}{dt} = -e_t^P(i,j) - \frac{ie_t^P(i,j)}{u_t^{PP}} \sum_{k,l\in\mathbb{N}} ke_t^P(k,l);\ \forall i,j\in\mathbb{N}; \tag{A.2}$$

$$\frac{de_t^S(i,j)}{dt} = -\frac{2ie_t^S(i,j)}{u_t^{PS}} \sum_{k,l\in\mathbb{N}} le_t^P(k,l);\ \forall i,j\in\mathbb{N}; \tag{A.3}$$

$$\frac{du_t^{PP}}{dt} = -2\sum_{k,l\in\mathbb{N}} ke_t^P(k,l); \tag{A.4}$$

$$\frac{du_t^{PS}}{dt} = -2\sum_{k,l\in\mathbb{N}} le_t^P(k,l); \tag{A.5}$$

where

$$a_0^P = 0;$$

$$e_0^P(i,j) = \frac{\mu(i,j)}{N_P};\ \forall i,j\in\mathbb{N} \text{ and } e_0^S(i,j) = \frac{\nu(i,j)}{N_s};\ \forall i,j\in\mathbb{N};$$

$$u_0^{PP} = \frac{1}{N_P}\sum_{i=0}^{\infty}\sum_{i=0}^{\infty} i\mu(i,j) \text{ and } u_0^{PS} = \frac{1}{N_P}\sum_{i=0}^{\infty}\sum_{i=0}^{\infty} 2j\mu(i,j).$$

Defining $h_t(i,j) = e^t e_t^P(i,j)\forall i,j\in\mathbb{N}$ and introducing a new time variable τ_t such that $\frac{d\tau_t}{dt} = \frac{\sum_i\sum_j ie_t^P(i,j)}{u_t^{PP}}$; it is possible to decouple the system of equations (A.2) and (A.4). Please note that the mapping $t\to\tau_t$ is a bijection of $[0,\infty)$ onto $[0,\tau_\infty)$ (the detail explanation and justification of this time transformation can

be found in [10]). In order to simplify the notation, in the following calculus we will drop the time dependence in τ_t: $\tau_t = \tau$.

Working with the rescaled time variables: $u_\tau^{PP} = u_{t(\tau)}^{PP}$ and $h_\tau(i,j) = h_{t(\tau)}(i,j); \forall i,j \in \mathbb{N}$, we can obtain the following system of differential equations:

$$\frac{du_\tau^{PP}}{d\tau} = -2u_\tau^{PP}; \tag{A.6}$$

$$\frac{dh_\tau(i,j)}{d\tau} = -ih_\tau(i,j); \forall i,j \in \mathbb{N}; \tag{A.7}$$

where

$$u_0^{PP} = \frac{1}{N_P}\sum_{i=0}^{\infty}\sum_{i=0}^{\infty} i\mu(i,j) \text{ and } h_0(i,j) = e_0^P(i,j); \forall i,j \in \mathbb{N}.$$

The system has the following unique solution:

$$u_\tau^{PP} = u_0^{PP}e^{-2\tau}; \tag{A.8}$$

$$h_\tau(i,j) = h_0(i,j)e^{-i\tau}. \tag{A.9}$$

By $h_\tau(i,j)$ definition, we have that

$$e_\tau^P(i,j) = e^{-t}e_0^P(i,j)e^{-i\tau}; \forall i,j \in \mathbb{N}. \tag{A.10}$$

Substituting Eqs. (A.8), (A.9) and (A.10) in τ definition, we obtain

$$\frac{d\tau_t}{dt} = e^{-t}\frac{\sum_i\sum_j ie_0(i,j)e^{-i\tau}}{u_\tau^{pp}}, \tag{A.11}$$

that represents the transformation between τ and t and vice versa. τ_∞ is obtained from Eq. (A.11) by solving:

$$\int_0^{\tau_\infty} \frac{u_0^{PP}e^{-2\sigma}}{\sum_i\sum_j ie_0^P(i,j)e^{-i\sigma}}d\sigma = 1. \tag{A.12}$$

Working with the rescaled time $e_\tau^S(i,j)$ and once u_τ^{PS} is totally determined with Eq. (A.5) and Eq. (A.10), we have that

$$e_\tau^S(i,j) = e_0^S(i,j)\left(\frac{u_\tau^{PS}}{u_0^{PS}}\right)^i; \forall i,j \in \mathbb{N}, \tag{A.13}$$

where

$$u_\tau^{PS} = u_0^{PS} + \int_0^\tau -2\sum_i\sum_j je_0^P(i,j)e^{-i\sigma}\frac{u_0^{PP}e^{-2\sigma}}{\sum_i\sum_j ie_0^P(i,j)e^{-i\sigma}}d\sigma \tag{A.14}$$

□

Appendix B. A Proof of Theorem 4

Defining the normalized processes $\tilde{A}_t^S = A_t^S/N_S$, $\tilde{E}_t^S(j) = E_t^S(j)/N_S$, and $\tilde{U}_t^{SS} = U_t^{SS}/N_S$. Then, as $N_S \to \infty$, they converge in probability to the solution of the following set of differential equations:

$$\frac{da_t^S}{dt} = \sum_{l\in\mathbb{N}} e_t^S(l); \tag{B.1}$$

$$\frac{de_t^S(j)}{dt} = -e_t^S(j) - \frac{je_t^S(j)}{u_t^{SS}}\sum_{l\in\mathbb{N}} le_t^S(l); \forall j \in \mathbb{N}; \tag{B.2}$$

$$\frac{du_t^{SS}}{dt} = -2\sum_{l\in\mathbb{N}} le_t^S(l); \tag{B.3}$$

where

$$a_0^S = 0;$$
$$e_0^S(j) = \sum_{k\in\mathbb{N}} e_\infty^S(k,j)\ \forall j \in \mathbb{N}$$
$$u_0^{SS} = \frac{1}{N_S}\sum_{l\in\mathbb{N}} l\nu(k,l);$$

By similar manipulations of the differential equations, defining $h_t(j) = e^t e_t^S(j) \forall j \in \mathbb{N}$ and using the analogous definition of τ_t as in Theorem 2, we have:

$$u_\tau^{SS} = u_0^{SS}e^{-2\tau}; \tag{B.4}$$

$$e_\tau^S(j) = e^{-t}e_0^S(j)e^{-j\tau}; \forall i,j \in \mathbb{N}; \tag{B.5}$$

where

$$\frac{d\tau_t}{dt} = \frac{\sum_j je_t^S(j)}{u_t^{SS}}. \tag{B.6}$$

We are interested on the limit of a_t^S as t goes to infinity (when the secondary sensing phase is over). Please note that it is the same as τ goes to τ_∞, being τ_∞ the solution of:

$$\int_0^{\tau_\infty} \frac{u_0^{SS}e^{-2\sigma}}{\sum_{l\in\mathbb{N}} le_0^S(l)e^{-l\sigma}}d\sigma = 1. \tag{B.7}$$

Then, working with Eq. (B.1), the proportion of active secondary transmitters converges in probability to:

$$a_\infty^S = \int_0^{\tau_\infty}\sum_{j\in\mathbb{N}} e_0^S(j)e^{-j\tau}\frac{u_0^{SS}e^{-2\tau}}{\sum_{j\in\mathbb{N}} je_0^S(j)e^{-j\tau}}d\tau \tag{B.8}$$

□